A pathogenic C terminus-truncated polycystin-2 mutant enhances receptor-activated Ca2+ entry via association with TRPC3 and TRPC7.

メタデータ	言語: eng
	出版者:
	公開日: 2017-10-03
	キーワード (Ja):
	キーワード (En):
	作成者:
	メールアドレス:
	所属:
URL	http://hdl.handle.net/2297/48418

A Pathogenic C Terminus-truncated Polycystin-2 Mutant Enhances Receptor-activated Ca²⁺ Entry via Association with TRPC3 and TRPC7*[S]

Kyoko Miyagi[‡1], Shigeki Kiyonaka[§¶1], Kazunori Yamada[‡], Takafumi Miki[§], Emiko Mori[§], Kenta Kato[§],
Tomohiro Numata[§], Yuichi Sawaguchi[§], Takuro Numaga[§], Toru Kimura[∥], Yoshikatsu Kanai[∥**], Mitsuhiro Kawano[‡],
Minoru Wakamori[§], Hideki Nomura[‡‡], Ichiro Koni[‡], Masakazu Yamagishi[‡], and Yasuo Mori[§¶2]

From the §Department of Synthetic Chemistry and Biological Chemistry, Graduate School of Engineering, Kyoto University and
¶CREST, Japan Science and Technology Agency, Kyoto 615-8510, the ‡Division of Rheumatology, Department of Internal Medicine,
Kanazawa University Graduate School of Medicine and ‡‡Department of General Medicine, Kanazawa University Hospital,
Kanazawa 920-8641, the ∥Department of Pharmacology and Toxicology, School of Medicine, Kyorin University, Tokyo 181-8611,
and the **Department of Pharmacology, Graduate School of Medicine, Osaka University, Osaka 565-0871, Japan

Mutations in *PKD2* gene result in autosomal dominant polycystic kidney disease (ADPKD). *PKD2* encodes polycystin-2 (TRPP2), which is a homologue of transient receptor potential (TRP) cation channel proteins. Here we identify a novel *PKD2* mutation that generates a C-terminal tail-truncated TRPP2 mutant 697fsX with a frameshift resulting in an aberrant 17-amino acid addition after glutamic acid residue 697 from a family showing mild ADPKD symptoms. When recombinantly expressed in HEK293 cells, wild-type (WT) TRPP2 localized at the endoplasmic reticulum (ER) membrane significantly enhanced Ca²⁺ release from the ER upon muscarinic acetylcholine receptor (mAChR) stimulation. In contrast, 697fsX, which showed a predominant plasma membrane localization characteristic of TRPP2 mutants with C terminus deletion, prominently increased mAChR-activated Ca²⁺ influx in cells expressing TRPC3 or TRPC7. Coimmunoprecipitation, pulldown assay, and cross-linking experiments revealed a physical association between 697fsX and TRPC3 or TRPC7. 697fsX but not WT TRPP2 elicited a depolarizing shift of reversal potentials and an enhancement of single-channel conductance indicative of altered ion-permeating pore properties of mAChR-activated currents. Importantly, in kidney epithelial LLC-PK1 cells the recombinant 679fsX construct was codistributed with native TRPC3 proteins at the apical membrane area, but the WT construct was distributed in the basolateral membrane and adjacent intracellular areas. Our results suggest that heteromeric cation channels comprised of the TRPP2 mutant and the TRPC3 or TRPC7 protein induce enhanced receptor-activated Ca²⁺ influx that may lead to dysregulated cell growth in ADPKD.

Autosomal dominant polycystic kidney disease (ADPKD)[3] is a genetically heterogeneous Mendelian inheritance disorder affecting ~1 in 1000 live births (1). ADPKD is characterized clinically by progressive formation and enlargement of renal cysts that demonstrate abnormalities in cell growth, fluid secretion, and extracellular matrix with other common complications (2). Linkage analyses have shown that either *PKD1* or *PKD2* loci are responsible for almost all ADPKD pedigrees. Nearly 85% of ADPKD pedigrees have been linked to *PKD1*, and ~15% have been linked to *PKD2* (2, 3). In *PKD2* cases end-stage renal disease develops at a mean age of 10–15 years later than in *PKD1* cases, although heterogeneity in clinical phenotype is seen among *PKD2* mutations (4).

The *PKD2* gene, consisting of 15 exons, encodes a 968-amino acid integral transmembrane protein polycystin-2 (PC2, TRPP2) (5). Recent reports suggested that the C terminus of TRPP2 interacts with the coiled-coil domain of the *PKD1* gene product, polycystin-1 (PC1) (6). TRPP2 has homology to polycystin-L (TRPP3) (7), another member of the polycystin superfamily that has been shown to conduct Ca²⁺-permeable cation currents (8–10), and to a family of transient receptor potential (TRP) channels as well as voltage-gated Ca²⁺ channels, which raises the possibility that TRPP2 mediates transmembrane Ca²⁺ fluxes (3, 5) as a member of the TRP subfamily, TRP"P". Invertebrate and vertebrate TRP homologues of the so-called "canonical" TRPC subfamily are characterized by activation induced upon stimulation of phospholipase C-coupled receptors (11). TRPC channels have been originally proposed as store-operated channels activated by Ca²⁺ depletion of stores, whereas closely related TRPC homologues, TRPC3, TRPC6, and TRPC7, showed activation sensitivity to the membrane-delimited action of diacylglycerol (12–14). Notably, an *Orai* family distinct from TRPs had recently emerged as a major molecular entity for store-operated channel subtypes (15).

[3] The abbreviations used are: ADPKD, autosomal dominant polycystic kidney disease; PC2, polycystin-2; PC1, polycystin-1; TRP, transient receptor potential; TRPC, TRP canonical; ER, endoplasmic reticulum; mAChR, muscarinic acetylcholine receptor; CCh, carbachol; PM, plasma membrane; WT, wild type; EGFP, enhanced green fluorescent protein; RIPA buffer, radioimmune precipitation assay buffer; GST, glutathione *S*-transferase; ERK, extracellular signal-regulated kinase.

Thus, members of the TRPC family, which form homomeric or heteromeric channels different in their function and regulation (16), are currently the best candidates for receptor stimulation-activated Ca^{2+} entry channels.

Different types of *PKD2* mutations include nonsense mutations and frameshift-inducing deletions/insertions that result in truncation of the TRPP2 protein sequence (17, 18). The physiological function of TRPP2 and pathogenesis of TRPP2 mutations have been explained by seemingly conflicting hypotheses, particularly with regard to the truncation mutations that generate aberrant TRPP2 proteins lacking the C-terminal tail (6, 19–29). Hanaoka *et al.* (6) suggested that PC1 and TRPP2 coassemble at the plasma membrane (PM) to produce a new channel and regulate renal tubular morphology and function. Nauli *et al.* (20) proposed that PC1 and TRPP2 form mechanosensitive channels in the primary cilium of kidney cells. Naturally occurring pathogenic mutations of TRPP2, which disrupt their associations through their C-terminal tails (30), result in the defect in translocation of TRPP2 to PM. In contrast, a role of TRPP2 as a subunit of intracellular channels with the endoplasmic reticulum (ER)-targeting sequence, whose deletion induces trafficking to PM in pathogenic *PKD2* mutants, has been suggested (26, 27). Another possibility is that TRPP2 functions appropriately both as Ca^{2+} release channels in ER and, under certain defined conditions, as PM Ca^{2+} entry channels (31). However, it is still unclear how the C terminus-truncated TRPP2 mutant proteins behave after being mistranslocated from ER to the PM independently of the interaction with PC1. Thus, the physiological function of normal and pathogenic mutant TRPP2 as well as its operating subcellular site is yet to be established.

In the present study we have identified a novel *PKD2* gene mutation (2092delA) that generates a TRPP2 product (697fsX) with a frameshift resulting in an aberrant 17-amino acid addition after glutamic acid residue 697 (Glu^{697}) at the C terminus in a Japanese family. The recombinant TRPP2 mutant 697fsX was examined for subcellular localization as well as molecular and functional properties in HEK293 cells. 697fsX localized at the PM elicited a physical association with the TRPC3 or TRPC7 protein and muscarinic acetylcholine receptor (mAChR)-activated Ca^{2+} influx in HEK293 cells coexpressing TRPC3 or TRPC7, whereas wild-type (WT) TRPP2 localized at the ER significantly enhanced mAChR-activated Ca^{2+} release. In polarized kidney epithelial LLC-PK1 cells, confocal image analysis revealed codistribution of native TRPC3 with transfected 697fsX in the apical membrane but not with WT TRPP2 distributed in the basolateral membrane area. These observations suggest dual impacts of *PKD2* mutations producing TRPP2 proteins deleted with the C-terminal tail in the pathogenesis of ADPKD.

EXPERIMENTAL PROCEDURES

Patients—After informed consent had been obtained, the proband diagnosed with polycystic kidney disease and his living family members were assessed by abdominal ultrasonography and clinical evaluation including routine laboratory tests of renal and liver function. The criteria for the diagnosis of ADPKD were based on the studies of Bear *et al.* (32). Individuals were considered to be affected if they were found to have at least one cyst in each kidney and at least two cysts in one kidney. Abdominal computed tomography imaging was performed using Hi Speed Advantage (GE Medical Systems).

Linkage Analysis—Genomic DNAs were extracted from peripheral blood leukocytes of the family members from whom informed consent had been obtained, according to standard procedures (33). Linkage analysis was performed using four CA-repeat markers for the *PKD1* locus (D16S521, D16S3024, D16S3027, D16S423) and four for the *PKD2* locus (D4S2964, D4S1534, D4S414, D4S1572) as described elsewhere (34). AmpliTaq gold DNA polymerase (PerkinElmer Life Sciences) and a universal touch-down thermal cycling program with GeneAmp PCR System Model 9600 (PE Applied Biosystems) was applied. Amplified products, distinguishable by their fluorescent wavelength and size, were loaded onto a 30-cm-long non-denaturing 10% polyacrylamide gel. After gel electrophoresis for 3 h at 25 watts, the data were analyzed with Genescan software (PerkinElmer Life Sciences) to obtain exact genosizes (35). Logarithm of odds scores were calculated with the M-Link program of the Linkage package Version 5.2 (36).

PKD2 Gene Sequencing—PCR of exons 1–15 was performed using AmpliTaq (PerkinElmer Life Sciences) or LATaq (Takara) as recommended by the manufacturer. The specific primers, annealing temperatures, and cycling conditions were as described before (37). The amplified PCR products containing exons after purification by Microcon-PCR (Millipore) were sequenced in both directions on an automatic fluorescence sequencer (ABM Prism 310 DNA sequencer, Applied Biosystems) using the Dye terminator thermal cycle sequence kit (Amersham Biosciences).

cDNA Cloning and Plasmid Construction—Full-length *PKD2* cDNA was generated by ligation of two cDNA fragments; a PCR fragment spanning nucleotide residues 52–614 of published *PKD2* cDNA sequence (5) and the cDNA clone lacking 5′-terminal ~0.5 kbp obtained by screening human kidney oligo-(dT)-primed cDNA library with human EST R48321 as a probe. The fragments were subsequently subcloned into pEGFP-C (Clontech) or pCMV-tag2 (Stratagene) with the untranslated leader sequence as described previously (14). The 697fsX and R742X constructs were created by using PCR. Mouse TRPC1-C7 cDNAs (38) were subcloned into pCI-neo (Promega), pEGFP-N (Clontech), or pDsRed-Monomer-N (Clontech) by using PCR. GenBank accession numbers are NM_011643 (TRPC1), NM_011644 (TRPC2), NM_019510 (TRPC3), AF190646 (TRPC4), AF029983 (TRPC5), NM_013838 (TRPC6), and AF139923 (TRPC7). Pore mutants of 697fsX (697fsX(E648Q), 697fsX(E650Q), 697fsX(E651Q)) and of TRPC3 (TRPC3(E632Q)) were created by using PCR.

Cell Cultures and cDNA Expression—HEK293 cells were cultured in Dulbecco's modified Eagle's medium containing 10% fetal bovine serum, 30 units/ml penicillin, and 30 μg/ml streptomycin. HEK293 cells were cotransfected with the recombinant plasmids and pEGFP-F (Clontech) as a transfection marker (39). Transfection was carried out using SuperFect Transfection Reagent (Qiagen) or the calcium phosphate precipitation method. Cotransfection efficiency was estimated to be 91.7 ± 1.7%. LLC-PK1 cells were cultured in Dulbecco's

modified Eagle's medium containing 10% fetal bovine serum, 30 units/ml penicillin, and 30 μg/ml streptomycin. To establish LLC-PK1 lines stably expressing EGFP-WT or EGFP-697fsX, LLC-PK1 cells were transfected with pEGFPN1-TRPP2 or pEGFPN1-TRPP2(697fsX) using SuperFect and cultured in Dulbecco's modified Eagle's medium containing Geneticin (1 mg/ml) (Sigma) for selection.

Fluorescent Measurement of $[Ca^{2+}]_i$ Changes—After 36 h of transfection using SuperFect, cells were plated onto poly-L-lysine-coated glass coverslips and subjected to measurement 6–16 h after plating on the coverslips. The cells on coverslips were loaded with fura-2 in Dulbecco's modified Eagle's medium containing 1 μM fura-2/AM (Dojindo Laboratories), 10% fetal bovine serum, 30 units/ml penicillin, and 30 μg/ml streptomycin at 37 °C for 40 min and washed with HEPES buffer saline containing 107 mM NaCl, 6 mM KCl, 1.2 mM MgSO$_4$, 2 mM CaCl$_2$, 11.5 mM glucose, and 20 mM HEPES (the pH was adjusted to 7.4 with NaOH). The coverslips were then plated in a perfusion chamber mounted on the stage of the microscope. Fluorescence images of the cells were recorded and analyzed with a video image analysis system (ARGUS CA-20 or AQUA-COSMOS; Hamamatsu Photonics) as described previously (38). All ratio data were calculated to $[Ca^{2+}]_i$ using an *in vivo* calibration method (38). The later phase of $[Ca^{2+}]_i$ was measured at 700 s.

Confocal Visualization of Fluorescent Fusion Constructs and Immunofluorescent Cell Staining—After 36 h of transfection using SuperFect, HEK293 cells were plated onto poly-L-lysine-coated glass base dishes (IWAKI) and subjected to measurement 6–16 h after plating on the dishes.

LLC-PK1 cells stably expressing EGFP-WT or EGFP-697fsX were grown on Transwell filters (24 mm, 0.4-mm pore polycarbonate, Corning) for 5–7 days, and media were changed every 2 days. Cells were fixed with 4% paraformaldehyde and then permeabilized with 0.1% Triton X-100. The cells were incubated with primary antibodies followed by subsequent incubation with the anti-rabbit Cy3-conjugated secondary antibody. Primary antibodies were anti-TRPC3 (38) and monoclonal acetylated α-tubulin (6-11B-1, Sigma). Fluorescence images were acquired with a confocal laser-scanning microscope (Olympus FV500) using the 488-nm line of an argon laser for excitation and a 505–525-nm band-pass filter for emission (EGFP) or the 543-nm line of a HeNe laser for excitation and a 560-nm long-pass filter for emission (DsRed monomer or Cy3). The specimens were viewed at high magnification using plan oil objectives (60×, 1.40 numerical aperture, Olympus).

Coimmunoprecipitation and Western Blotting Analysis—After 48 h of transfection using SuperFect, HEK293 cells were solubilized in RIPA buffer (pH 8.0) containing 0.1% SDS, 0.5% sodium deoxycholate, 1% Nonidet P-40, 150 mM NaCl, 50 mM Tris-HCl, 1 mM phenylmethylsulfonyl fluoride, and 10 μg/μl leupeptin or in IP-500 buffer (pH 7.5) containing 1% Triton X-100, 0.5% Nonidet P-40, 500 mM NaCl, 10 mM Tris-HCl, 1 mM EGTA, 1 mM EDTA, 10% sucrose, 1 mM phenylmethylsulfonyl fluoride, and 10 μg/μl leupeptin, then centrifuged at 17,400 × g for 20 min to remove cell debris. For coimmunoprecipitation, the cell lysate was incubated with anti-FLAG M2 monoclonal antibody (Sigma) for 2 h. Then the immunocom-

plexes were incubated with protein A-agarose beads (Santa Cruz) for 1 h, and the beads were washed with RIPA buffer. Immunoprecipitated proteins were fractionated by 10% SDS-PAGE and electrotransferred onto a nitrocellulose membrane. The blots were incubated with living colors polyclonal antibody (Clontech) or anti-TRPC3 and visualized using the ECL system (Amersham Biosciences).

Glutathione S-Transferase (GST) Pulldown—cDNAs for TRPC3 fragments and GST were subcloned into the pET23 vector (Novagen). All GST fusion proteins were expressed in *Escherichia coli* (Rosetta strain, Novagen) and affinity-purified using glutathione-Sepharose 4B beads (GE Healthcare). Cell lysate from HEK293 cells transiently expressing EGFP-679fsX was incubated with glutathione-Sepharose beads bound with GST fusion TRPC3 subfragments for 1 h, then the beads were washed with RIPA buffer at 4 °C. The proteins retained on the beads were characterized by Western blotting using living colors polyclonal antibody.

Purification of TRPC3 Complex and Chemical Cross-linking—After 48 h of transfection using the calcium phosphate precipitation method, HEK293 cells were homogenized with a Potter Teflon homogenizer in phosphate buffer saline at 4 °C. Cell debris was eliminated from the homogenate by centrifuging at 10,000 × g for 15 min. The supernatant was recentrifuged at 100,000 × g for 1 h to sediment membrane fractions.

The membrane fraction was solubilized in phosphate-based RIPA buffer (pH 8.0) containing 0.1% SDS, 0.5% sodium deoxycholate, 1% Nonidet P-40, 150 mM NaCl, 50 mM sodium phosphate, 1 mM phenylmethylsulfonyl fluoride, and 10 μg/μl leupeptin. After centrifuging at 100,000 × g for 30 min, the supernatant was incubated with anti-FLAG M2 affinity agarose (Sigma). The beads were washed twice with 10 bed volumes of phosphate-based RIPA buffer. Bound proteins were eluted with the buffer containing 100 μg/ml FLAG peptide (Sigma). The eluate was concentrated with a Microcon centrifuge filter unit YM-100 (Millipore). For chemical cross-linking, glutaraldehyde was then added to the final concentration of 12 mM at 4 °C for 1 h. The cross-linking reaction was terminated by incubation with an equal volume of SDS sample buffer 25 °C for 1 h, and the product was analyzed by Western blotting. A protein sample treated similarly, but without glutaraldehyde, was prepared as a control.

Electrophysiology—After cotransfection with pCI-neo-TRPC3 and pEGFP-C plasmids containing the cDNA for WT or 697fsX TRPP2, coverslips with cells were placed in dishes containing the solutions. Currents were recorded at room temperature (22–25 °C) using a whole-cell mode of the patch clamp technique with an EPC-9 patch clamp amplifier (HEKA Elektronik) or Axopatch 200B (Axon Instruments) as described previously (14). Patch pipettes were made from borosilicate glass capillaries (1.5-mm outer diameter; Hilgenberg) using a model P-87 Flaming-Brown micropipette puller (Sutter Instrument Co.). Pipette resistance ranged from 2 to 6 megaohms when filled with the pipette solutions described below. The series resistance was electronically compensated to >50%. Currents were sampled at 1 or 20 kHz after low pass filtering at 2.9 or 5 kHz in the experiments. Data acquisition was performed using the PULSE program (Version 7.5, HEKA Elektronik) or the

Clampex program (Version 10.2, Axon Instruments). Whole-cell currents were recorded in an external solution that contained 140 mM NaCl, 5 mM KCl, 2 mM $CaCl_2$, 1 mM $MgCl_2$, 10 mM HEPES, and 10 mM glucose (the pH was adjusted to 7.4 with NaOH). Current-voltage (*I-V*) relationships were obtained using a 500-ms positive voltage ramp from -120 to $+100$ mV. For the experiment to determine permeation selectivity, currents were recorded in external solutions that contained 140 mM CsCl, 10 mM HEPES, 10 mM glucose, and 20 mM mannitol (the pH was adjusted to 7.4 with CsOH) for Cs^+ external solutions, 140 mM NaCl, 10 mM HEPES, 10 mM glucose, and 26 mM mannitol (the pH was adjusted to 7.4 with NaOH) for Na^+ external solutions, and 50 mM $CaCl_2$, 40 mM HCl, 10 mM HEPES, 10 mM glucose, and 75 mM mannitol (the pH was adjusted to 7.4 with NMDG) for Ca^{2+} external solution. The pipette solution contained 95 mM cesium aspartate, 40 mM CsCl, 4 mM $MgCl_2$, 5 mM EGTA, 2 mM Na_2ATP, 5 mM HEPES, and 8 mM creatine phosphate (the pH was adjusted to 7.2 with CsOH). The single-channel amplitude and zero-current level were determined by eye using cursors. The open probability (NP_O; N is the number of channels in the *patch*, and Po is the single-channel open probability) recorded from cell-attached mode was calculated for a series of 50-ms test pulses to -160 or $+140$ mV. The NPo of single-channels was calculated by averaging NPo for 100 sweeps in the patches containing active channels. Single-channel currents were recorded in an external solution that contained 143 mM KCl, 2 mM $CaCl_2$, 1 mM $MgCl_2$, 2 mM KH_2PO_4, 10 mM HEPES, and 6 mM glucose (the pH was adjusted to 7.4 with KOH). The pipette solution contained 140 mM NaCl, 10 mM HEPES, and 10 mM glucose (the pH was adjusted to 7.4 with NaOH). Test solution was topically applied using the so-called "Y-tube" fast solution exchange device.

Statistical Analysis—All data are expressed as the mean ± S.E. The statistical analyses were performed using Student's *t* test.

RESULTS

Haplotype Analysis of PKD1 and PKD2 Gene—The male proband suffered from intracranial subarachnoidal hemorrhage from a ruptured cerebrovascular aneurysm, requiring neurosurgery, at the age of 65. Closer medical examination of the proband including abdominal computed tomography scanning revealed multiple cysts in both kidneys and liver (Fig. 1) with normal renal function, leading to a diagnosis of polycystic kidney disease. As indicated in Fig. 2, abdominal ultrasonography and laboratory tests of his living family members clarified that five family members including the proband had polycystic kidney disease according to the Bear *et al.* criteria (32). Liver cysts were observed in all five affected members. Some had hematuria, and the proband had a ruptured cerebral aneurysm, whereas there was no known family history of end stage renal disease.

By haplotype analysis with microsatellite markers shown in Fig. 2*A*, all affected members shared the haplotype against *PKD2* indicated in Fig. 2*B* (see the *shaded numbers*), but not *PKD1*, strongly suggesting that the ADPKD phenotype of the pedigree is positively linked to *PKD2* locus. Maximum logarithm of odds score against *PKD2* was 0.95 at D4S1572 followed
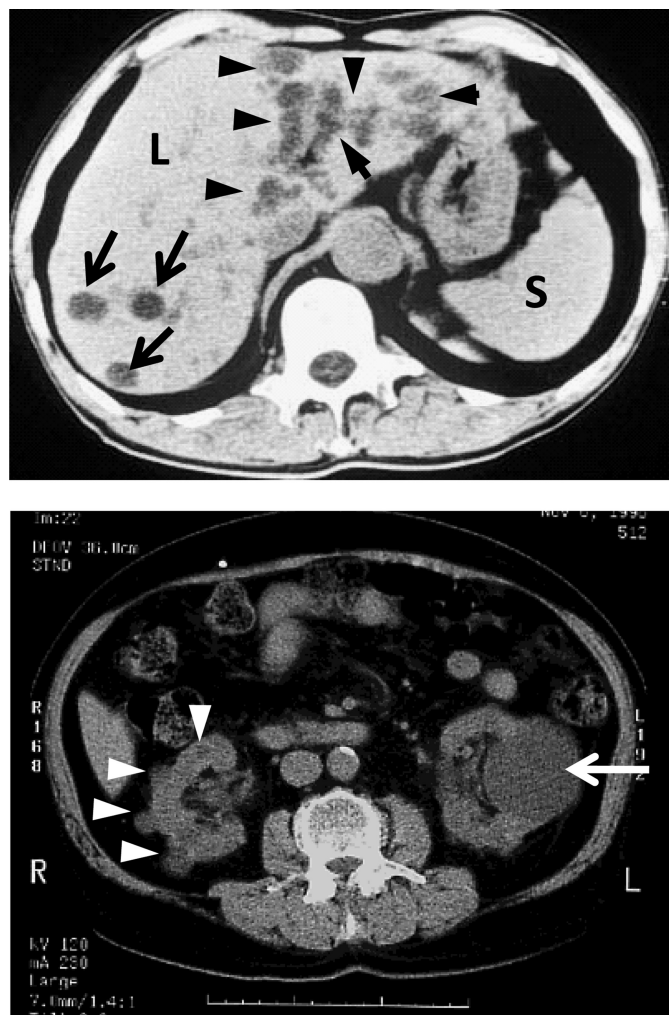

FIGURE 1. **Abdominal axial computed tomography scan of the proband.** *Top,* typical intrahepatic cysts (*black arrows*) and probable peribiliary cysts (*black arrowheads*) are seen. *Bottom,* computed tomography scan obtained inferior to *A* depicts multiple cysts in the bilateral kidneys, a large cyst on the *left* (*white arrow*), and the multiple small cysts on the *right* (*white arrowheads*). *L*, liver; *S*, spleen.

by 0.93 at D4S1534 and 0.90 at D4S414 when $\theta = 0$ (Table 1), which were close to the theoretical maximum values obtained for this pedigree. The logarithm of odds scores for linkage between chromosome 16p markers and ADPKD were not informative.

The Novel PKD2 Mutation Generates an Aberrant 17 Amino Acid Sequence after Glu^{397} of TRPP2—DNA sequence analysis of the 15 exons in the *PKD2* gene undertaken in the proband revealed heterozygous single deletion at exon 10 (2092delA) (Fig. 3). This novel mutation caused a frameshift in the coding nucleotide sequence and is predicted to result in the addition of aberrant 17 amino acid residues WNSQILSERATIKLWSN after Glu^{697} of TRPP2 (697fsX). The sequence examination of the *PKD2* gene for his family members confirmed that 2092delA was cosegregated with the disease phenotype.

WT TRPP2 but Not 697fsX Enhances Ca^{2+} Release from ER—When recombinantly expressed in HEK293 cells, the 697fsX TRPP2 mutant was predominantly localized in the PM area, in contrast to the WT TRPP2 distributed intracellularly in ER (Fig. 4*A*). The M_3 receptor has been reported as an endoge-

A

Ch 16

D16S521
D16S3024
PKD1
D16S3027
D16S423
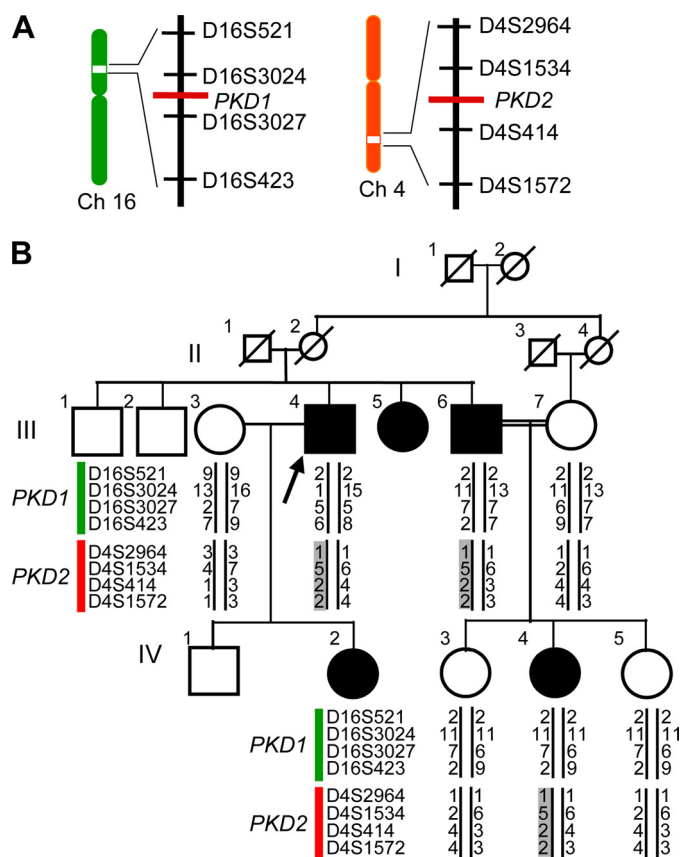
Ch 4

D4S2964
D4S1534
PKD2
D4S414
D4S1572

B

FIGURE 2. **Linkage analysis of the pedigree.** *A*, shown is a schematic representation of the chromosomal regions containing the *PKD1* and *PKD2* loci. *B*, shown is a pedigree structure of the family. An *arrow* indicates the proband. *Circles* and *squares* represent females and males, respectively. All affected members are indicated by *closed symbols*, and all unaffected individuals are indicated by *open symbols*. A *diagonal line through the symbol* indicates that the individual is deceased. *Numbers below the symbols* indicate allele numbers of each microsatellite marker shown in *A*. Allele numbers are codominant alleles at a single locus. The numbers run consecutively from 1 to the maximum number of alleles observed. The phenotype consists of two allele numbers corresponding to a genotype. Haplotypes with *shaded numbers* indicate affected (five in generation III and two in generation IV are not analyzed).

TABLE 1
Logarithm of odds scores for linkage between ADPKD and each microsatellite maker of the pedigree

Locus	Recombination fraction (θ)						
	0	0.02	0.04	0.06	0.08	0.1	0.2
D16S521	−1.41					−0.42	−0.19
D16S3024	0.18	0.16	0.14	0.12	0.10	0.09	0.03
D16S3027	0.15	0.13	0.10	0.09	0.08	0.06	0.01
D16S423	0.52	0.48	0.45	0.41	0.38	0.34	0.19
D4S2964	0.10	0.10	0.09	0.09	0.08	0.08	0.05
D4S1534	0.93	0.89	0.84	0.80	0.75	0.70	0.47
D4S414	0.90	0.86	0.82	0.78	0.73	0.69	0.47
D4S1572	0.95	0.90	0.86	0.81	0.77	0.72	0.48

nous mAChR subtype in HEK293 cells (40). Upon stimulation of endogenous mAChR by 30 μM carbachol (CCh), cytosolic Ca^{2+} concentration ($[Ca^{2+}]_i$) rises were significantly enhanced by WT TRPP2 expression in HEK293 cells, whereas CCh-induced $[Ca^{2+}]_i$ rises in 697fsX-expressing cells were indistinguishable from those in vector-transfected control HEK293 cells (Fig. 4*B*). This enhancement of mAChR-activated Ca^{2+} responses by WT is attributable to increased Ca^{2+} release from stores, as $[Ca^{2+}]_i$ rises elicited by CCh stimulation after omis-

sion of external Ca^{2+} were enhanced significantly by WT but not by 697fsX (Fig. 4*C*). In contrast, Ca^{2+} entry, observed as $[Ca^{2+}]_i$ rises which are elicited by readministration of external Ca^{2+} under constant CCh stimulation, was enhanced slightly but significantly by 697fsX but not by WT. Interestingly, thapsigargin-induced Ca^{2+} entry was indistinguishable between control and TRPP2-expressing cells (Fig. 4*D*). When high K^+ (30 mM)-containing solution was employed to establish depolarizing experimental conditions, enhancements of Ca^{2+} release and Ca^{2+} entry, respectively, by WT and 697fsX were still observed, suggesting that the effects of constructs are not due to membrane potential changes (supplemental Fig. 1). Thus, WT and 697fsX exert contrasting impacts on mAChR-activated $[Ca^{2+}]_i$ rises; WT may enhance Ca^{2+} release induced by inositol 1,4,5-trisphosphate, whereas 697fsX may increase Ca^{2+} entry, activated via mechanisms presumably independent of store depletion. In HEK293 cells reverse transcription-PCR analysis showed endogenous expression of PC1, TRPP2, TRPC1, TRPC3, TRPC4, and TRPC6 (supplemental Fig. 2), which may contribute to the enhancement of Ca^{2+} release by WT and Ca^{2+} influx by 697fsX mutant.

Association of 697fsX with TRPC3 or TPRC7 Enhances CCh-induced Ca^{2+} Influx—To characterize targets of action of 697fsX in enhancing receptor-activated Ca^{2+} entry, TRPP2 constructs were tested in HEK293 cells coexpressing TRPC homologues, which have been reported as receptor-activated Ca^{2+}-permeable channels coupled to phospholipase C activation and inositol 1,4,5-trisphosphate production (12–14). The enhancing effect of 697fsX on CCh-induced Ca^{2+} responses was significantly pronounced by TRPC3 or TRPC7 coexpression (Fig. 5, *A* and *B*), resulting in significant augmentation of sustained $[Ca^{2+}]_i$ rises attributable to Ca^{2+} entry, observed in the later phase (Fig. 5*A*) or after readdition of external Ca^{2+} (Fig. 5*C*). The 697fsX effect is not due to membrane potential changes, because augmentation of Ca^{2+} influx by coexpressing 697fsX with TRPC3 was observed under high K^+ (30 mM) conditions (supplemental Fig. 3). The 697fsX effect is not attributable to protein expression levels of TRPCs, because protein expression levels were comparable between 697fsX-sensitive and -insensitive TRPCs when FLAG- or EGFP-tagged constructs were assessed by Western blotting analysis (supplemental Fig. 4). As observed above in Fig. 4*B*, WT TRPP2 enhanced peak $[Ca^{2+}]_i$ rises regardless of the presence of external Ca^{2+} in TRPC3-expressing cells, supporting enhancement of inositol 1,4,5-trisphosphate-induced Ca^{2+} release by WT TRPP2 (Fig. 5, *A* and *C*).

697fsX but Not WT TRPP2 Interacts with TRPC3 or TPRC7—We used immunoprecipitation to test whether 697fsX forms a protein complex with TRPC3 or TRPC7. HEK293 cells coexpressing TRPP2 and TRPC constructs were solubilized in Nonidet P-40/deoxycholate/SDS-based stringent RIPA lysis buffer or Nonidet P-40/Triton X-100-based high salt IP-500 buffer (41). Western blotting analysis indicated that the TRPC3-EGFP and TRPC7-EGFP constructs were coimmunoprecipitated with FLAG-697fsX but not with FLAG-WT TRPP2 by anti-FLAG antibody under both conditions (Fig. 6*A*, supplemental Fig. 5). In contrast to TRPC3 and TRPC7, TRPC1 showed coimmunoprecipitation with both WT (41) and the 697fsX mutant.
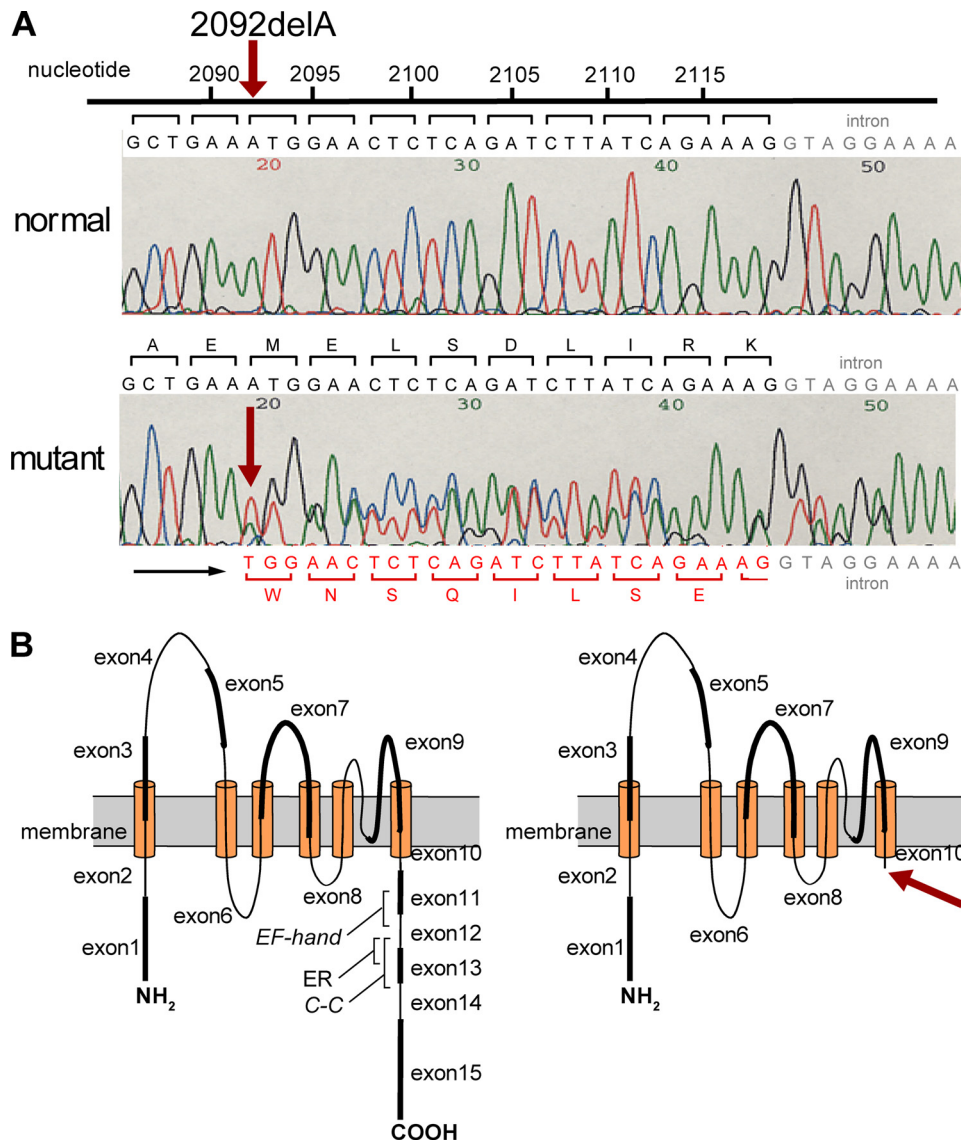
FIGURE 3. **Sequencing analysis of genomic PCR products showing the *PKD2* mutation 2092delA.** *A, arrows* indicate the PKD2 mutation 2092delA. The sequence of the normal allele is shown *above* the electropherograms of the control, and the mutant sequence is *below* the patient tracing. The sample reveals a heterozygous mutation for a single adenosine deletion at nucleotide 2092 on exon 10. *B,* shown is a schematic illustration of WT (*left*) and the 697fsX mutant protein with a truncation of cytoplasmic C-terminal region (*arrow*) (*right*). *ER,* endoplasmic reticulum retention signal; *EF-hand,* Ca^{2+} binding domain, *C-C,* coiled-coil domain.

eluted with 100 μg/ml FLAG. Then the purified proteins were cross-linked by glutaraldehyde, and the product was analyzed by Western blotting. The band of TRPC3 was shifted to an upward position by the cross-linking, which corresponds well with the size of the tetramer (Fig. 6*C, left*) (42). Importantly, a protein band of cross-linked EGFP-697fsX copurified with TRPC3-FLAG using anti-FLAG agarose was similar in size to the cross-linked TRPC3 (Fig. 6*C, right*). Although exact protein stoichiometry of complex formation was not determined, it can be estimated that the content of 697fsX is low compared with that of TRPC3, as efficiency of cross-linking of EGFP-697fsX with TRPC3-FLAG (Fig. 6*C, right*) is not as high as that between TRPC3-FLAG proteins (Fig. 6*C, left*). These results suggest that TRPC3 and 697fsX form heteromeric protein complex.

Furthermore, confocal images demonstrated overlapping localization of EGFP-697fsX with coexpressed TRPC3-DsRed monomer near the PM area (Fig. 6*D*). However, WT showed no significant colocalization with coexpressed TRPC3. In polarized kidney epithelial LLC-PK1 cells, native TRPC3 was colocalized with transfected EGFP-697fsX in the apical membrane area but not with WT TRPP2 distributed in the basolateral membrane and adjacent intracellular areas (Fig. 7). The results suggest that 697fsX localized at the PM enhances receptor-activated Ca^{2+} influx through physical association with TRPC3 or TRPC7. Interestingly, WT TRPP2 and the C-terminal-truncated 697fsX mutant were distributed in cilia in polarized LLC-PK1 as previously reported for TRPP2 WT and the L703X mutant (supplemental Fig. 8) (43).

697fsX Modifies Ion Permeation Properties of TRPC3—To directly investigate the functional impacts of 697fsX on TRPC3-mediated Ca^{2+} entry, ionic currents were examined using the whole-cell mode of the patch clamp method (Fig. 8). At a holding potential (V_h) of −60 mV, 697fsX but not WT TRPP2 significantly augmented inward currents evoked by stimulation with 60 μM CCh in TRPC3-expressing cells (TRPC3 plus WT, 2.5 ± 0.8 pA/picofarad (pF), n = 6; TRPC3 plus 697fsX, 7.3 ± 1.0 pA/pF, n = 16; TRPC3 plus vector, 3.7 ± 0.8 pA/pF, n = 5) (Fig. 8, *A* and *B*), consistent with the above $[Ca^{2+}]_i$ measurements. *I-V* relationships showed a prominent

In vitro pulldown assays using GST fusion constructs identified the amino acid residues 659–753 carrying the TRPC EWKFAR motif as a 697fsX-interacting domain in the TRPC3 protein (Fig. 6*B,* supplemental Fig. 6). In addition, the previous reported C terminus-truncated mutant R742X (5) also showed coimmunoprecipitation with TRPC3 (supplemental Fig. 7), excluding the possibility that aberrant amino acid sequences attached at the C-terminal end of truncated mutants play important roles in associating with TRPC3 and TRPC7. To further confirm protein multimerization of TRPC3 with 697fsX, a chemical cross-linking method was employed. From the membranes of HEK293 cells transiently expressing TRPC3-FLAG and EGFP-697fsX, protein complexes were solubilized with phosphate-based RIPA buffer and purified using immunoaffinity techniques. Protein complexes including TRPC3-FLAG were trapped to anti-FLAG agarose and were competitively
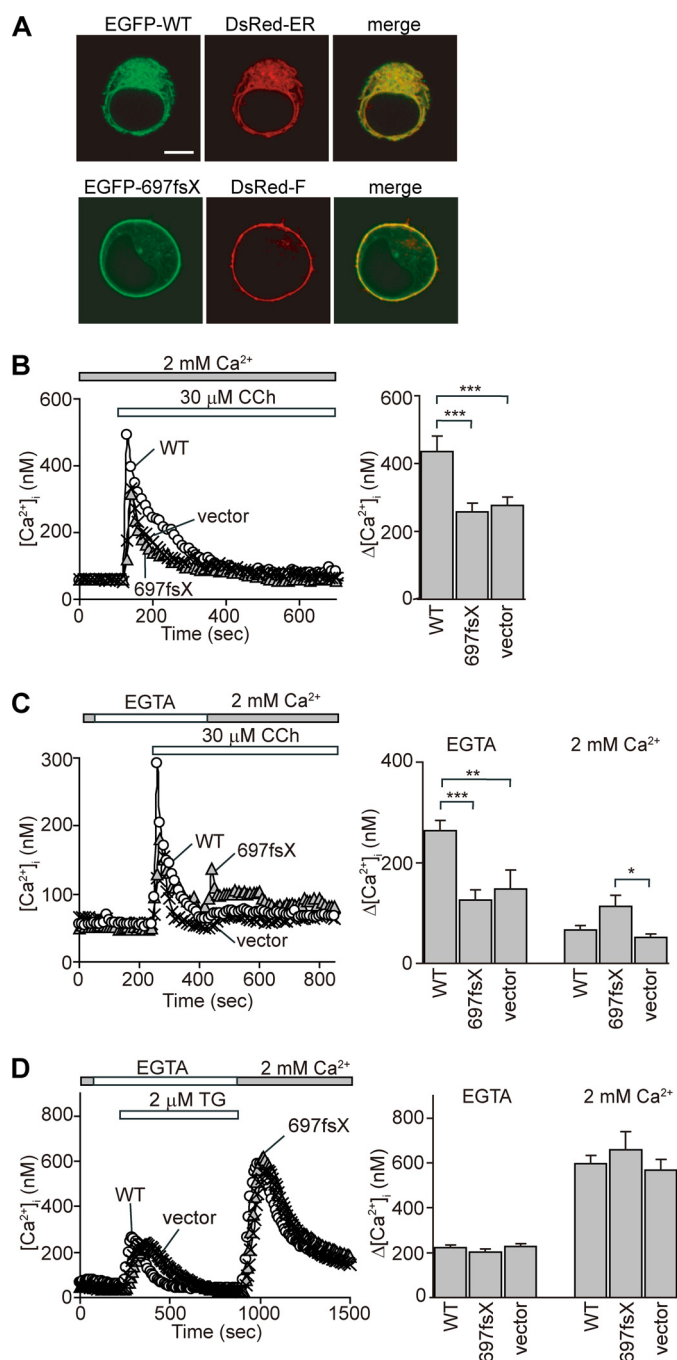
FIGURE 4. **Subcellular localization and functional impacts of WT and the 697fsX TRPP2 mutant on [Ca²⁺]ᵢ in HEK293 cells.** *A*, confocal fluorescent imaging reveals the concentration of 697fsX at the PM and that of WT at the ER. *Upper*, EGFP-tagged WT colocalized with the ER marker DsRed-ER is shown. *Lower*, EGFP-tagged 697fsX colocalized with the PM marker DsRed-F is shown. The *bar* indicates 10 μm. *B*, WT enhances Ca²⁺ responses upon mAChR stimulation by CCh. *Left*, average time courses are shown. *Right*, peak [Ca²⁺]ᵢ rises (n = 23–35). *C*, WT and 697fsX enhance Ca²⁺ release and Ca²⁺ entry, respectively, upon mAChR stimulation. *Left*, average time courses are shown. *Right*, peak [Ca²⁺]ᵢ rises in Ca²⁺-free solution and after Ca²⁺ readmministration (n = 27–36) are shown. *D*, thapsigargin (*TG*)-induced, store-operated Ca²⁺ entry is unaffected by WT or 697fsX. *Left*, average time courses are shown. *Right*, peak [Ca²⁺]ᵢ rises in Ca²⁺-free solution and after Ca²⁺ readmministration (n = 25–33) are shown. Significance of differences: *, $p < 0.05$; **, $p < 0.01$l; ***, $p < 0.001$.

FIGURE 5. **Functional association of 697fsX with TRPC3 and TRPC7 proteins promotes mAChR-evoked Ca²⁺ responses.** *A*, 697fsX enhances mAChR-evoked Ca²⁺ responses in TRPC3-expressing HEK293 cells. *Left*, average time courses are shown. *Right*, peak [Ca²⁺]ᵢ rises and [Ca²⁺]ᵢ rises in the later phase (700 s) (n = 25–36) are shown. *B*, peak mAChR-activated [Ca²⁺]ᵢ rises in the cells expressing respective TRPC1-C7 channels with or without 697fsX (n = 23–48) are shown. *C*, coexpression of 697fsX with TRPC3 significantly enhances mAChR-evoked Ca²⁺ responses attributable to Ca²⁺ entry upon readdition of extracellular Ca²⁺. *Left*, average time courses are shown. *Right*, peak [Ca²⁺]ᵢ rises in Ca²⁺-free solution and after Ca²⁺ readministration (n = 29–37) are shown. Significance of differences: **, $p < 0.01$; ***, $p < 0.001$.

rectification at depolarizing potentials as previously reported for receptor-activated TRPC3 currents (Fig. 8C) (44). Currents induced by 1-oleoyl-2-acetyl-*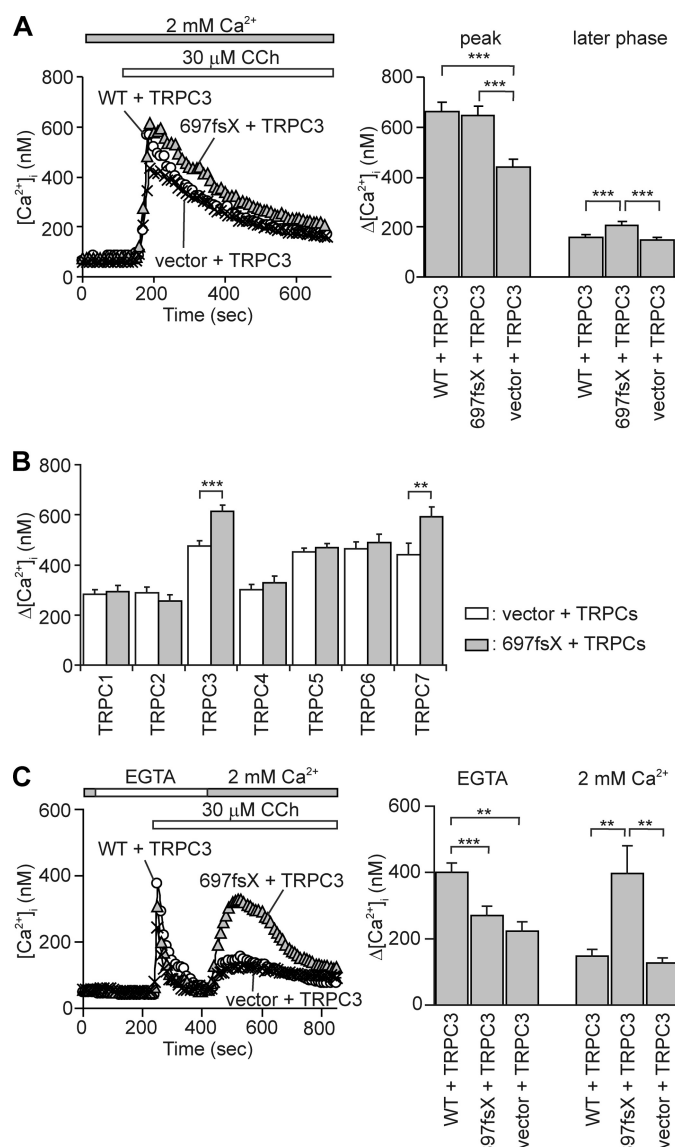sn*-glycerol, the membrane-per-meable analogue of the physiological TRPC3 activation trigger diacylglycerol, were augmented in HEK293 cells coexpressing TRPC3 with 697fsX compared with cells expressing TRPC3 with WT or vector control (supplemental Fig. 9). As indicated in Fig. 8C, 697fsX significantly shifted reversal potential toward depolarizing potentials compared with WT and vector control. To quantitatively evaluate the cation selectivity of cation channels formed in HEK293 cells, extracellular Cs⁺ was replaced with Na⁺ or Ca²⁺. The ratio of permeability of different ions to that of intracellular Cs⁺ was calculated from changes in reversal potential brought about by ion replacement using equations derived from the Goldman-Hodgkin-Katz equations for the
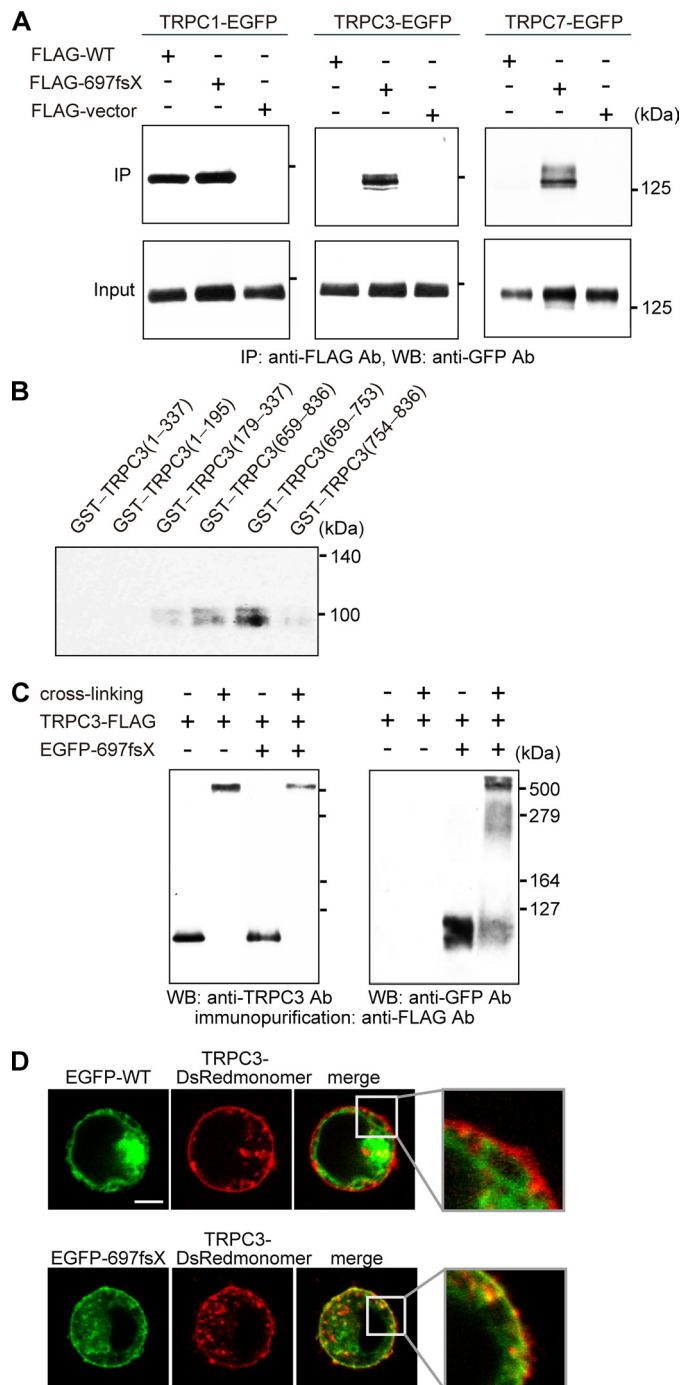
FIGURE 6. Physical association of 697fsX with TRPC3 or TRPC7. *A,* shown is coimmunoprecipitation of TRPC3-EGFP or TRPC7-EGFP with FLAG-697fsX in stringent RIPA lysis buffer. Immunoprecipitates (*IP*) with anti-FLAG antibody (*Ab*) are separated on 10% SDS-PAGE and blotted with anti-GFP antibody in Western blotting analysis (*WB*) to detect the EGFP fusion constructs. *B,* shown is a pulldown assay of 697fsX with GST fusion TRPC3 subfragments. GST fusion proteins immobilized on glutathione-Sepharose beads are incubated with cell lysates obtained from EGFP-697fsX-transfected HEK293 cells. Bound proteins are analyzed by Western blot using an antibody for GFP. *C,* chemical cross-linking of TRPC3 and 697fsX is shown. Immunoaffinity-purified protein samples using anti-FLAG antibody are reacted with 12 mM glutaraldehyde, and reaction products are separated by SDS-PAGE followed by WB using antibody for TRPC3 (*left*) or GFP (*right*). *D,* overlapping subcellular distribution of EGFP-697fsX with TRPC3-DsRed monomer in the PM area is shown. Confocal images of HEK293 cells coexpressing EGFP-WT plus TRPC3-DsRed monomer (*upper*) or EGFP-697fsX plus TRPC3-DsRed monomer (*lower*) are shown. EGFP-697fsX merges well with TRPC3-DsRed monomer in PM. The *bar* indicates 10 μm.
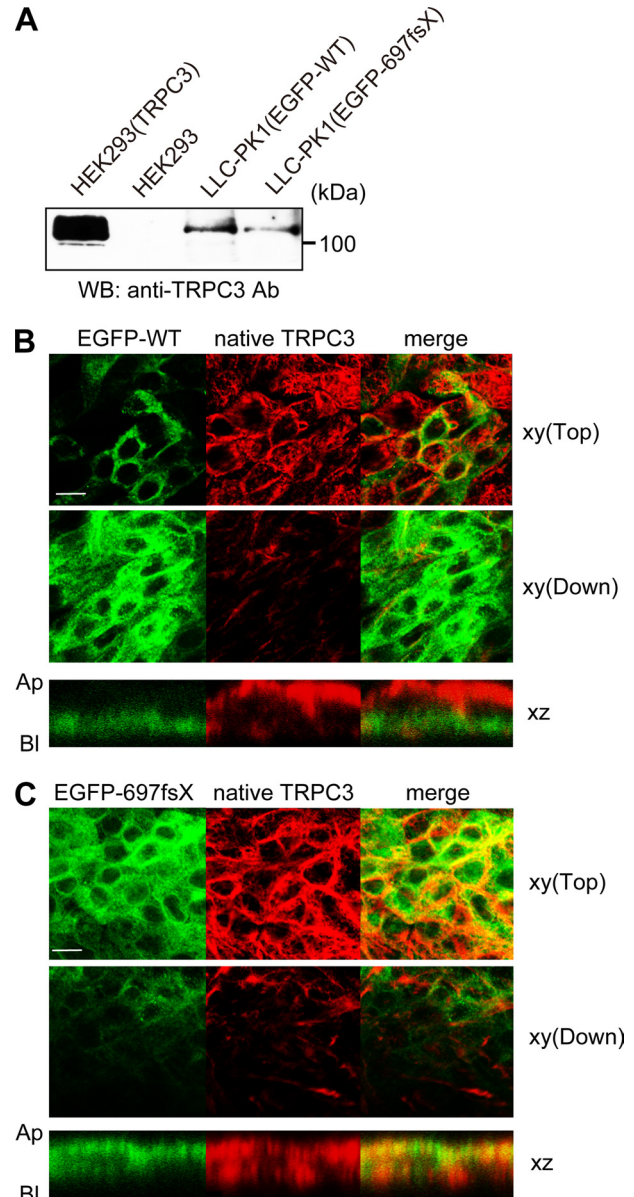

FIGURE 7. Native TRPC3 is colocalized with EGFP-697fsX but not with EGFP-WT in polarized LLC-PK1 cells. *A,* expression of native TRPC3 in LLC-PK1 cells transfected with EGFP-TRPP2 fusion constructs is shown. Western blotting analysis (*WB*) is performed using anti-TRPC3 antibody. Nontransfected and TRPC3-transfected HEK293 cells are shown as controls. *B* and *C,* shown is confocal imaging of LLC-PK1 cells stably expressing EGFP-WT or EGFP-697fsX grown in Transwell filters. Cells were fixed with paraformaldehyde and immunostained with anti-TRPC3 antibody. Serial confocal sections were collected from the top to the bottom of cell monolayers. The *bar* indicates 10 μm. *Ab,* antibody; *Ap,* apical; *Bl,* basolateral.

biionic conditions (14). The values of P_{Na}/P_{Cs} and P_{Ca}/P_{Cs} were 0.93 ± 0.01 and 1.08 ± 0.06 for TRPC3 plus WT ($n = 7$), 0.93 ± 0.01 and 1.10 ± 0.09 for TRPC3 plus vector ($n = 6$), and 0.97 ± 0.01 and 1.15 ± 0.08 for TRPC3 plus 697fsX ($n = 7$, $p < 0.05$ *versus* WT and vector for P_{Na}/P_{Cs}). The data are indicative of an increase in permeation selectivity to Na$^+$ for TRPC3 plus 697fsX.

The single-channel recording of the cell-attached mode revealed an increment of single-channel conductance for 697fsX by 50-ms step pulses at −160 mV from a V_h of 0 mV but not for WT TRPP2 or vector by stimulation with 60 μM CCh in
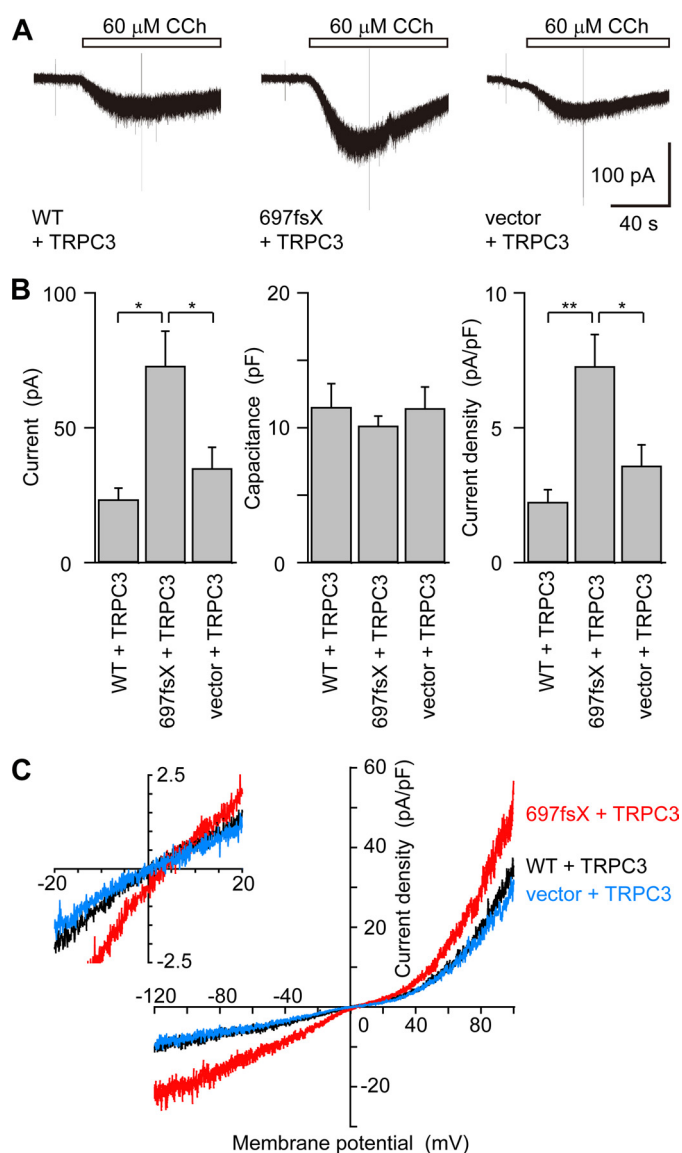
FIGURE 8. **Functional association of 697fsX with mAChR-activated TRPC3 channels.** *A*, shown are representative trace of ionic currents recorded from HEK293 cells expressing TRPC3 with WT (*left*), 697fsX (*middle*), or vector (*right*) at a V_h of −60 mV. *B*, shown are peak current amplitudes (*left*), cell capacitances (*middle*), and current densities (*right*) of the CCh-activated currents at a V_h of −60 mV ($n = 5$–16). Current density corresponding to the amount of current applied per unit area is obtained by dividing the current amplitude by the cell capacitance. *C*, representative *I-V* relations of the CCh-activated currents, obtained by subtracting currents before activation of channels from those after activation from *A* (*inset*, expanded traces around the reversal potentials). A 500-ms positive voltage ramp from −120 mV to +100 mV is applied. Reversal potentials of CCh-induced currents; +1.9 ± 1.9 mV for WT ($n = 6$), +0.1 ± 2.6 mV for vector ($n = 5$), and +7.3 ± 1.0 mV for 697fsX ($n = 16$, $p < 0.05$ *versus* WT and vector). Significance of differences: *, $p < 0.05$; **, $p < 0.01$.

FIGURE 9. **TRPC3 coexpressed with the 697fsX elicits an altered single-channel amplitude.** *A*, representative traces are shown of single-channel currents recorded in cell-attached mode from HEK293 cells expressing TRPC3 with WT TRPP2 (*left*), 697fsX (*middle*), or vector (*right*) at −160 mV. CCh was added in the bath solution. *Dashed lines* represent different closing or opening states of single channels. *C* represents the closing state; O_1 and O_2 represent the vector plus TRPC3 and 697fsX plus TRPC3 opening states, respectively. *B*, amplitudes of the CCh-activated single-channel currents at −160 mV ($n = 25$–29). TRPC3 plus WT, −15.6 ± 0.3 pA ($n = 25$); TRPC3 plus 697fsX, −16.9 ± 0.4 pA ($n = 28$); TRPC3 plus vector, −15.1 ± 0.3 pA ($n = 29$). Significance of differences: *, $p < 0.05$.

TRPC3-expressing cells (TRPC3 plus WT, −15.6 ± 0.3 pA, $n = 25$; TRPC3 plus 697fsX, −16.9 ± 0.4 pA, $n = 28$; TRPC3 plus vector, −15.1 ± 0.3 pA, $n = 29$) (Fig. 9). Sixty μM CCh or 10 μM 1-oleoyl-2-acetyl-*sn*-glycerol failed to induce any detectable changes in current traces in cells expressing 697fsX or WT TRPP2 alone (data not shown, $n = 6$). We also studied the effect of pore mutations in TRPC3 or 697fsX on ion conduction. For TRPC3, a negatively charged residue in the putative selective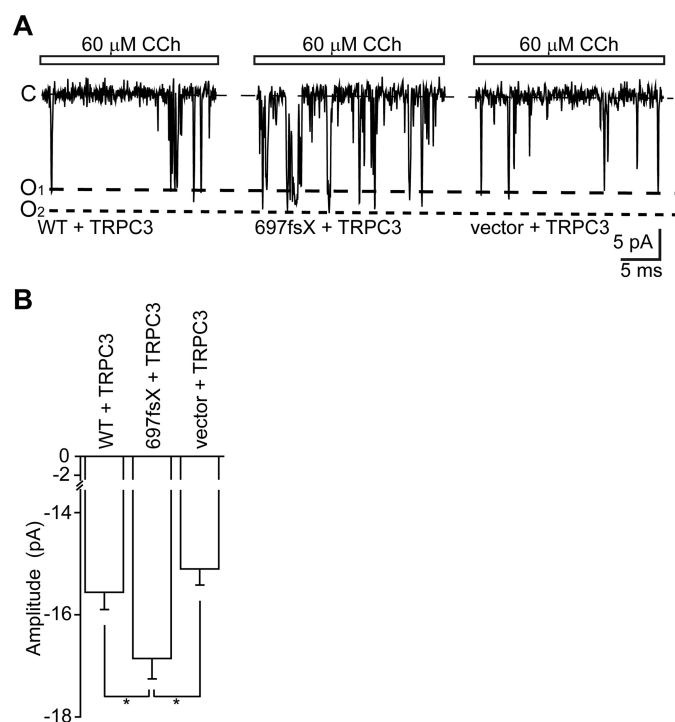 filter (45) was replaced with a neutral residue (TRPC3(E632Q)) (supplemental Fig. 10). For 679fsX, respective negatively charged residues between putative pore helix and the S6 transmembrane were replaced with a neutral residue (697fsX(E648Q), 697fsX(E650Q), and 697fsX(E651Q)) (45, 46). Single-channel current amplitudes were compared at +140 mV (50 ms), because this strong depolarizing potential gave higher single-channel activity of TRPC3(E632Q), which allowed us to carry out better analyses upon stimulation with 60 μM CCh in TRPC3(E632Q)-transfected cells ($NP_O = 0.09 \pm 0.01$ in vector plus TRPC3(E632Q), $n = 29$) than −160 mV ($NP_O = 0.01$, $n = 29$). TRPC3 and TRPC3(E632Q) showed distinct single-channel current amplitudes (vector plus TRPC3, 14.3 ± 0.1 pA ($n = 38$); vector plus TRPC3(E632Q), 11.9 ± 0.4 pA ($n = 29$) (Fig. 10). In vector-transfected cells, similar single-channel currents were not detectable ($n = 6$). 697fsX increased amplitudes of single channels in TRPC3(E632Q)-expressing cells as well as in TRPC3-expressing cells to significantly different levels (697fsX plus TRPC3, 16.3 ± 0.1 pA ($n = 30$); 697fsX plus TRPC3(E632Q), 15.3 ± 0.2 pA ($n = 27$)) (Fig. 10*A*, *middle traces*). Compared with 697fsX combined with TRPC3, individual 697fsX mutants (697fsX(E648Q), 697fsX(E650Q), and 697fsX(E651Q)) combined with TRPC3 showed decreased single-channel conductance (697fsX(E648Q) plus TRPC3, 15.7 ± 0.1 pA ($n = 15$); 697fsX(E650Q) plus TRPC3, 15.5 ± 0.2 pA ($n = 24$); 697fsX(E651Q) plus TRPC3, 15.0 ± 0.2 pA ($n = 26$)). The pore mutants were also examined for divalent cation (Ca^{2+}
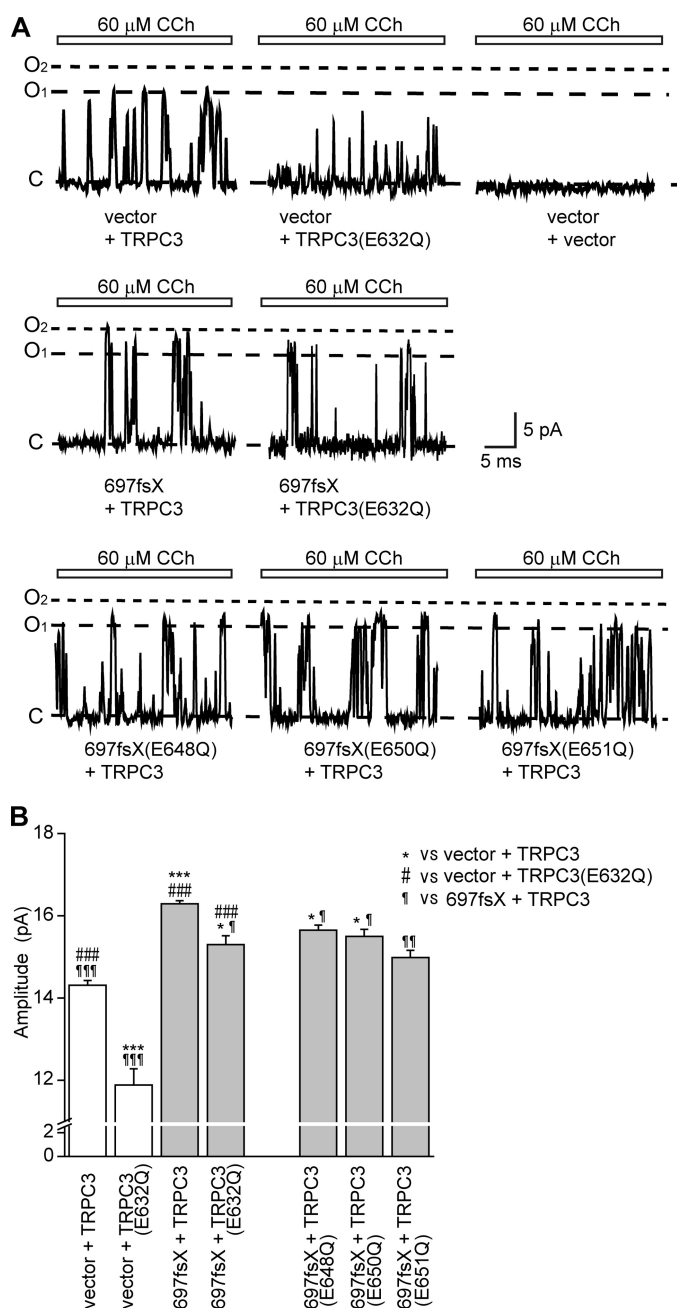
FIGURE 10. **TRPC3(E632Q) coexpressed with 697fsX or TRPC3 coexpressed with 697fsX mutants (E648Q, E650Q, or E651Q) also elicits an altered single-channel amplitude.** *A,* shown are representative traces of single-channel currents recorded in cell-attached mode from HEK293 cells expressing vector with TRPC3 (*upper left*), vector with TRPC3(E632Q) (*upper center*), vector with vector (*upper right*), 697fsX with TRPC3 (*middle left*), 697fsX with TRPC3(E632Q) (*middle center*), 697fsX(E648Q) with TRPC3 (*lower left*), 697fsX(E650Q) with TRPC3 (*lower center*), and 697fsX(E651Q) with TRPC3 (*lower right*) at +140 mV. Sixty μM CCh was added in the bath solution. *Dashed lines* represent different closing or opening states of single channels. *C* represents closing state; O_1 and O_2 represent the opening states of vector plus TRPC3 and 697fsX plus TRPC3, respectively. *B,* amplitudes of the CCh-activated single-channel currents at +140 mV are shown; vector plus TRPC3, 14.3 ± 0.1 pA ($n = 38$); vector plus TRPC3(E632Q), 11.9 ± 0.4 pA ($n = 29$); 697fsX plus TRPC3, 16.3 ± 0.1 pA ($n = 30$); 697fsX plus TRPC3(E632Q), 15.3 ± 0.2 pA ($n = 27$); 697fsX(E648Q) plus TRPC3, 15.7 ± 0.1 pA ($n = 15$); 697fsX(E650Q) plus TRPC3, 15.5 ± 0.2 pA ($n = 24$); 697fsX(E651Q) plus TRPC3, 15.0 ± 0.2 pA ($n = 26$). Data represent the mean ± S.E. For statistical assessment, multiple comparisons were conducted by analysis of variance followed by the Tukey-Kramer test. Significance of differences: *, $p < 0.05$; ***, $p < 0.001$ *versus* vector plus TRPC3; ###, $p < 0.001$ *versus* vector plus TRPC3(E632Q); ¶, $p < 0.05$; ¶¶, $p < 0.01$; ¶¶¶, $p < 0.001$ *versus* 697fsX plus TRPC3.

and Sr^{2+}) influx activity using fura-2 (supplemental Fig. 11). The E632Q mutation significantly suppressed both CCh-induced Ca^{2+} and Sr^{2+} influx via TRPC3 (supplemental Fig. 11, *A and B*). Notably, in TRPC3(E632Q)-expressing cells, coexpression of 697fsX enhanced Ca^{2+} influx but not Sr^{2+} influx (supplemental Fig. 11, *C and D*), suggesting a contribution of 697fsX to Ca^{2+} permeability of CCh-activated E632Q-containing channels. The pore mutations of 697fsX suppressed Ca^{2+} influx but not Sr^{2+} influx in cells coexpressing TRPC3 and 697fsX (supplemental Fig. 11, *E and F*). These results using pore mutants provide supportive evidence that coexpression of 697fsX and TRPC3 directs the formation of heteromeric channels carrying pore properties different from homomeric TRPC3 channels.

DISCUSSION

Coimmunoprecipitation, GST pulldown, and cross-linking experiments suggest that the C terminus-truncated TRPP2 mutant 697fsX undergoes physical association with TRPC3 and TRPC7. In electrophysiological recordings, coexpression of 697fsX but not that of WT TRPP2 caused a depolarizing shift of reversal potentials and an increased single-channel amplitude of mAChR-induced currents in TRPC3-expressing cells. These altered ion permeation properties of TRPC3-mediated cation currents after coexpression of 697fsX suggest that TRPC3 and 697fsX form heteromultimeric cation channels in which both TRPC3 and 697fsX function as pore-forming subunits, and pore-lining residues are different from those of homomultimeric TRPC3 channels. Consistent with this notion, HEK293 cells coexpressing 697fsX with WT TRPC3 and those with E632Q TRPC3 mutant showed single-channel currents with different amplitudes, excluding a possibility that TRPC3 proteins, which form channels independently of 697fsX proteins, support co-translocation of 697fsX via indirect mechanisms, for example, by sharing the same membrane microdomain.

Previously, the TRPP2 C-terminal tail containing the coiled-coil domain 772–796 was shown to be responsible for the assembly of TRPP2 with PC1 using the C-terminal tail-truncated mutant R742X (6). Because the coiled-coil domain is also deleted from the TRPP2 sequence in the 697fsX mutant, 697fsX can be incapable of forming a complex with PC1. In LLC-PK1 cells, native TRPC3 proteins were colocalized with transfected 697fsX in the apical membrane area but not with WT TRPP2 distributed in the basolateral membrane and adjacent intracellular areas (Fig. 7). Therefore, in native tissues of ADPKD patients with 697fsX, a deficiency of PC1 interaction can lead to the formation of heteromultimeric TRPP2/TRPC3 channels with ion permeation properties different from those of TRPC3-containing channels in normal tissues. Interestingly, cation influx activity is increased when 697fsX is coexpressed with TRPC3. It is, therefore, possible that 697fsX enhances trafficking of TRPC3 channels through protein multimerization, as previously reported for TRPV4 associated with TRPP2 (47). Other TRPP2-interacting proteins may also participate in trafficking of TRPP2 proteins (48–51).

TRPP2 abundantly expressed in ER membrane has been suggested to act as a Ca^{2+} release channel of intracellular stores

(26) and to functionally interact with inositol 1,4,5-trisphosphate receptor-induced Ca^{2+} release (52). TRPP2 is also reported to form protein complexes with PC1 or TRPC1 to induce Ca^{2+} influx at the PM (6, 41). However, because our data clearly indicate that overexpression of TRPP2 potentiates receptor-activated Ca^{2+} release but not Ca^{2+} influx in HEK293 cells, TRPP2 should mainly function as a Ca^{2+} release channel. In this study we detected endogenous expression of PC1, TRPP2, TRPC1, TRPC3, TRPC4, and TRPC6 in HEK293 cells (supplemental Fig. 2). Interestingly, our data suggest a higher expression level of TRPP2 compared with those of PC1 and TRPC1, further suggesting that endogenous PC1 and TRPC1 are fully associated with endogenous TRPP2 and that PC1 and TRPC1 are not freely accessible for recombinant TRPP2. With regard to the augmentation of Ca^{2+} influx in HEK293 cells recombinantly expressing 697fsX, endogenous TRPC3 but not TRPC7 was detected in HEK293 cells. Other TRPCs such as TRPC1, TRPC4, and TRPC6 are also endogenously expressed in HEK293 cells but fail to show enhancement of Ca^{2+} influx by 697fsX when recombinantly expressed (Fig. 5*B*). Therefore, endogenous TRPC3 may interact with 697fsX at the PM.

The present study reveals that the TRPP2 C terminus-truncating mutations exert a dual pathogenic impact at different subcellular sites, the ER and PM, on receptor-induced $[Ca^{2+}]_i$ mobilization. At the ER, the potentiation effect of WT TRPP2 on receptor-activated Ca^{2+} release from ER was abolished by the 697fsX mutation in HEK293 cells. This is consistent with the previous report of Cai *et al.* (27), which suggested that the C terminus-truncated mutation (R742X) abolishes retention of TRPP2 at the ER membrane, where TRPP2 regulates Ca^{2+} release (26). At the PM, physical and functional association of 697fsX TRPP2 proteins with TRPC3 or TRPC7 prominently enhanced receptor-activated Ca^{2+} entry into HEK293 cells. This finding clarifies the interaction target of C terminus-truncated TRPP2 proteins and their activation mechanism as ion channels, which were unresolved issues. Previous reports only described the disrupted assembly of TRPP2 with PC1 and consequent PM mistranslocation of TRPP2 by the R742X mutation (6) as well as the abnormal spontaneous $[Ca^{2+}]_i$-independent cation current via the R742X TRPP2 mutant (29). Furthermore, compared with the proposed loss of Ca^{2+} influx by ablation of the association between PC1 and TRPP2s, the enhanced Ca^{2+} influx via complexation with TRPC3 or TRPC7 proteins is a gain of function more likely consistent with the dominant phenotype of the *PKD* mutations. Thus, the obtained data may provide an important clue to address the discrepancy between seemingly conflicting hypotheses with regard to the subcellular sites of the pathogenic action of TRPP2 C terminus mutants (6, 26).

The present study also implies the biological context in which the C-terminal-truncated mutant channels function. The observed enhancement of receptor-induced Ca^{2+} entry via association of 697fsX with TRPC3 supports the contention that 697fsX induces dysregulated cell growth and death in ADPKD, as TRPC3 channels are indeed activated upon receptors such as B cell (38) and T cell receptors (53), and brain-derived neurotrophic factor receptors (54, 55) linked to cell growth and survival, and play an important role in cardiac hypertrophy (56–

59). Importantly, ADPKD is a systemic disorder with a variety of other manifestations including liver cysts, cerebral aneurysms, and various cardiac valvular abnormalities. Wide expression of TRPC3, TRPC7, and TRPP2 in various tissues including kidney (60–62) suggests that the pathogenic association between C terminal-truncated TRPP2s and TRPC3 or TRPC7 underlies the ADPKD abnormalities observed in multiple tissues (1). In normal tissues native TRPP2 and TRPC3 showed an interesting contrast in subcellular localization, with TRPP2 concentrated in the basolateral membrane and TRPC3 localized in the apical domain of rat tubular cells (61–65). Our observation (Fig. 7) is consistent with this localization pattern. In addition, basolateral localization of TRPC1 in MDCK cells (64) and its physical interaction with TRPP2 have been reported (41). Notably, during preparation of this manuscript, it has been reported that the heteromeric channels comprised of TRPP2 and TRPC1 are activated in response to receptor stimulation (66). It is, therefore, speculated that C-terminal truncations disrupt the PC1-TRPP2 assembly as well as the formation of heteromultimeric TRPC1/TRPP2 channels in the basolateral membrane (65). The heteromultimerization may consequently induce mislocalization of TRPP2 proteins and the formation of heteromultimeric TRPC3/TRPP2 channels in the apical membrane, finally leading to transduction of pathogenic signals in ADPKD tissues. Taking into consideration that TRPC3 and TRPC7 are different from TRPC1 in molecular and functional properties (11), a conclusion based on TRPC1 should not be directly extrapolated to TRPC3 and TRPC7. This is consistent with an idea that TRPP2 mutants associated with TRPC3 and TRPC7 indeed play unique pathophysiological roles in signal transduction. We can raise a different possibility that unknown regulatory mechanisms, which suppress the action of the TRPP2 C terminus, may induce translocation to the apical membrane and subsequent heteromultimerization with WT TRPP2 and TRPC3 also in normal tissues under certain cellular conditions. In this scenario it is conceivable that the 697fsX mutant is constantly present at the apical membrane to transmit constitutively active aberrant signals in ADPKD tissues.

At the cellular level ADPKD inherited in a dominant manner has been explained by a recessive mechanism, leading to the complete loss of function through somatic mutations in the normal *PKD2* allele (the two-hit model). However, TRPP2 (PC2) is frequently observed in renal cystic epithelium of human ADPKD, raising the possibility that deregulated activation of *PKD2* may be associated with the cystogenesis of human ADPKD (67, 68). Furthermore, *PKD2*-overexpressing transgenic mice showed a development of typical renal cysts and an increase of proliferation and apoptosis, which are reflective of the human ADPKD phenotype (68). The transgenic mice also showed up-regulation of B-Raf/mitogen-activated protein kinase/extracellular signal-regulated kinase kinase (MEK)/ERK sequential signaling, a possible molecular mechanism of cystogenesis (68). Strikingly, TRPC3-mediated Ca^{2+} influx has been shown to play essential roles in ERK activation in various cell types (38, 69, 70). Therefore, formation of heteromeric channels comprised of 697fsX and TRPC3 and possible up-regula-

tion of ERK activity through Ca^{2+} regulation may be sufficient to trigger renal cystogenesis.

ADPKD is often considered a disease of adults, but it is clear that it already begins in childhood. Renal cysts in children with ADPKD have been associated with a wide clinical spectrum ranging from a total absence of symptoms to massive renal enlargement, hypertension, oliguria, and pulmonary hypoplasia in newborns (71). In this context the seemingly delayed onset symptoms shown by the 697fsX family can be categorized as a manifestation of a milder type of polycystic kidney disease. Interestingly, abnormal $[Ca^{2+}]_i$ regulation associated with *PKD2* haploinsufficiency has been related to vascular abnormalities (72). Based on this report, we can speculate that 697fsX restores the dosage reduction due to haploinsufficiency; despite mislocalization of 697fsX-containing channels, 697fsX-mediated Ca^{2+} entry may incompletely but significantly compensate for the net reduction in $[Ca^{2+}]_i$ mobilization by supplementing partial Ca^{2+} entry and Ca^{2+} release via TRPP2, derived from the remaining normal allele in heterozygous persons. In contrast, those mutants truncated at the middle or on the N-terminal side of the transmembrane core may be inactive as functional Ca^{2+} entry channels and may act as dominant negative forms for gene products of the normal *PKD2* allele or for TRPC3 to worsen gene dosage insufficiency. Further studies are required to establish the relationship between mutant properties and the severity of ADPKD.

REFERENCES

1. Gabow, P. A. (1993) *N. Engl. J. Med.* **329,** 332–342
2. Harris, P. C., and Torres, V. E. (2009) *Annu. Rev. Med.* **60,** 321–337
3. Nilius, B., Owsianik, G., Voets, T., and Peters, J. A. (2007) *Physiol. Rev.* **87,** 165–217
4. Hateboer, N., v Dijk, M. A., Bogdanova, N., Coto, E., Saggar-Malik, A. K., San Millan, J. L., Torra, R., Breuning, M., and Ravine, D. (1999) *Lancet* **353,** 103–107
5. Mochizuki, T., Wu, G., Hayashi, T., Xenophontos, S. L., Veldhuisen, B., Saris, J. J., Reynolds, D. M., Cai, Y., Gabow, P. A., Pierides, A., Kimberling, W. J., Breuning, M. H., Deltas, C. C., Peters, D. J., and Somlo, S. (1996) *Science* **272,** 1339–1342
6. Hanaoka, K., Qian, F., Boletta, A., Bhunia, A. K., Piontek, K., Tsiokas, L., Sukhatme, V. P., Guggino, W. B., and Germino, G. G. (2000) *Nature* **408,** 990–994
7. Nomura, H., Turco, A. E., Pei, Y., Kalaydjieva, L., Schiavello, T., Weremowicz, S., Ji, W., Morton, C. C., Meisler, M., Reeders, S. T., and Zhou, J. (1998) *J. Biol. Chem.* **273,** 25967–25973
8. Chen, X. Z., Vassilev, P. M., Basora, N., Peng, J. B., Nomura, H., Segal, Y., Brown, E. M., Reeders, S. T., Hediger, M. A., and Zhou, J. (1999) *Nature* **401,** 383–386
9. Inada, H., Kawabata, F., Ishimaru, Y., Fushiki, T., Matsunami, H., and Tominaga, M. (2008) *EMBO Rep.* **9,** 690–697
10. Shimizu, T., Janssens, A., Voets, T., and Nilius, B. (2009) *Pflügers Arch.* **457,** 795–807
11. Abramowitz, J., and Birnbaumer, L. (2009) *FASEB J.* **23,** 297–328
12. Boulay, G., Zhu, X., Peyton, M., Jiang, M., Hurst, R., Stefani, E., and Birnbaumer, L. (1997) *J. Biol. Chem.* **272,** 29672–29680
13. Hofmann, T., Obukhov, A. G., Schaefer, M., Harteneck, C., Gudermann, T., and Schultz, G. (1999) *Nature* **397,** 259–263
14. Okada, T., Inoue, R., Yamazaki, K., Maeda, A., Kurosaki, T., Yamakuni, T., Tanaka, I., Shimizu, S., Ikenaka, K., Imoto, K., and Mori, Y. (1999) *J. Biol. Chem.* **274,** 27359–27370
15. Hogan, P. G., and Rao, A. (2007) *Trends Biochem. Sci.* **32,** 235–245
16. Ambudkar, I. S. (2006) *Trends Pharmacol. Sci.* **27,** 25–32
17. Torra, R., Viribay, M., Tellería, D., Badenas, C., Watson, M., Harris, P., Darnell, A., and San Millán, J. L. (1999) *Kidney Int.* **56,** 28–33
18. Hateboer, N., Veldhuisen, B., Peters, D., Breuning, M. H., San-Millán, J. L., Bogdanova, N., Coto, E., van Dijk, M. A., Afzal, A. R., Jeffery, S., Saggar-Malik, A. K., Torra, R., Dimitrakov, D., Martinez, I., de Castro, S. S,, Krawczak, M., and Ravine, D. (2000) *Kidney Int.* **57,** 1444–1451
19. Li, X., Luo, Y., Starremans, P. G., McNamara, C. A., Pei, Y., and Zhou, J. (2005) *Nat. Cell Biol.* **7,** 1202–1212
20. Nauli, S. M., Alenghat, F. J., Luo, Y., Williams, E., Vassilev, P., Li, X., Elia, A. E., Lu, W., Brown, E. M., Quinn, S. J., Ingber, D. E., and Zhou, J. (2003) *Nat. Genet.* **33,** 129–137
21. Yamaguchi, T., Wallace, D. P., Magenheimer, B. S., Hempson, S. J., Grantham, J. J., and Calvet, J. P. (2004) *J. Biol. Chem.* **279,** 40419–40430
22. Grimm, D. H., Karihaloo, A., Cai, Y., Somlo, S., Cantley, L. G., and Caplan, M. J. (2006) *J. Biol. Chem.* **281,** 137–144
23. Ma, R., Li, W. P., Rundle, D., Kong, J., Akbarali, H. I., and Tsiokas, L. (2005) *Mol. Cell. Biol.* **25,** 8285–8298
24. Luo, Y., Vassilev, P. M., Li, X., Kawanabe, Y., and Zhou, J. (2003) *Mol. Cell. Biol.* **23,** 2600–2607
25. Pennekamp, P., Karcher, C., Fischer, A., Schweickert, A., Skryabin, B., Horst, J., Blum, M., and Dworniczak, B. (2002) *Curr. Biol.* **12,** 938–943
26. Koulen, P., Cai, Y., Geng, L., Maeda, Y., Nishimura, S., Witzgall, R., Ehrlich, B. E., and Somlo, S. (2002) *Nat. Cell Biol.* **4,** 191–197
27. Cai, Y., Maeda, Y., Cedzich, A., Torres, V. E., Wu, G., Hayashi, T., Mochizuki, T., Park, J. H., Witzgall, R., and Somlo, S. (1999) *J. Biol. Chem.* **274,** 28557–28565
28. Wu, G., D'Agati, V., Cai, Y., Markowitz, G., Park, J. H., Reynolds, D. M., Maeda, Y., Le, T. C., Hou, H., Jr., Kucherlapati, R., Edelmann, W., and Somlo, S. (1998) *Cell* **93,** 177–188
29. Chen, X. Z., Segal, Y., Basora, N., Guo, L., Peng, J. B., Babakhanlou, H., Vassilev, P. M., Brown, E. M., Hediger, M. A., and Zhou, J. (2001) *Biochem. Biophys. Res. Commun.* **282,** 1251–1256
30. Tsiokas, L., Kim, E., Arnould, T., Sukhatme, V. P., and Walz, G. (1997) *Proc. Natl. Acad. Sci. U.S.A.* **94,** 6965–6970
31. Vassilev, P. M., Guo, L., Chen, X. Z., Segal, Y., Peng, J. B., Basora, N., Babakhanlou, H., Cruger, G., Kanazirska, M., Ye, Cp., Brown, E. M., Hediger, M. A., and Zhou, J. (2001) *Biochem. Biophys. Res. Commun.* **282,** 341–350
32. Bear, J. C., McManamon, P., Morgan, J., Payne, R. H., Lewis, H., Gault, M. H., and Churchill, D. N. (1984) *Am. J. Med. Genet.* **18,** 45–53
33. Konoshita, T., Miyagi, K., Onoe, T., Katano, K., Mutoh, H., Nomura, H., Koni, I., Miyamori, I., and Mabuchi, H. (2001) *Am. J. Kidney Dis.* **37,** 113–118
34. Onoe, T., Konoshita, T., Miyagi, K., Yamada, K., Mutoh, H., Koni, I., and Nomura, H. (2003) *Clin. Nephrol.* **59,** 406–414
35. Jeff, H., and Elizabeth, N. (1997) in *Current Protocols in Human Genetics,* pp. 2–19, John Wiley and Sons, Hoboken, NJ
36. Lathrop, G. M., and Lalouel, J. M. (1984) *Am. J. Hum. Genet.* **36,** 460–465
37. Hayashi, T., Mochizuki, T., Reynolds, D. M., Wu, G., Cai, Y., and Somlo, S. (1997) *Genomics* **44,** 131–136
38. Nishida, M., Sugimoto, K., Hara, Y., Mori, E., Morii, T., Kurosaki, T., and Mori, Y. (2003) *EMBO J.* **22,** 4677–4688
39. Jurman, M. E., Boland, L. M., Liu, Y., and Yellen, G. (1994) *Biotechniques* **17,** 876–881
40. Jerman, J. C., Brough, S. J., Prinjha, R., Harries, M. H., Davis, J. B., and Smart, D. (2000) *Br. J. Pharmacol.* **130,** 916–922
41. Tsiokas, L., Arnould, T., Zhu, C., Kim, E., Walz, G., and Sukhatme, V. P. (1999) *Proc. Natl. Acad. Sci. U.S.A.* **96,** 3934–3939
42. Mio, K., Ogura, T., Hara, Y., Mori, Y., and Sato, C. (2005) *Biochem. Biophys. Res. Commun.* **333,** 768–777
43. Geng, L., Okuhara, D., Yu, Z., Tian, X., Cai, Y., Shibazaki, S., and Somlo, S. (2006) *J. Cell Sci.* **119,** 1383–1395
44. Trebak, M., St. J. Bird, G., McKay, R. R., Birnbaumer, L., and Putney, J. W., Jr. (2003) *J. Biol. Chem.* **278,** 16244–16252
45. Owsianik, G., Talavera, K., Voets, T., and Nilius, B. (2006) *Annu. Rev.*

Physiol. **68,** 685–717

46. Numata, T., and Okada, Y. (2008) *Channels* **2,** 283–286

47. Köttgen, M., Buchholz, B., Garcia-Gonzalez, M. A., Kotsis, F., Fu, X., Doerken, M., Boehlke, C., Steffl, D., Tauber, R., Wegierski, T., Nitschke, R., Suzuki, M., Kramer-Zucker, A., Germino, G. G., Watnick, T., Prenen, J., Nilius, B., Kuehn, E. W., and Walz, G. (2008) *J. Cell Biol.* **182,** 437–447

48. Köttgen, M., Benzing, T., Simmen, T., Tauber, R., Buchholz, B., Feliciangeli, S., Huber, T. B., Schermer, B., Kramer-Zucker, A., Höpker, K., Simmen, K. C., Tschucke, C. C., Sandford, R., Kim, E., Thomas, G., and Walz, G. (*2005*) *EMBO J.* **24,** 705–716

49. Lehtonen, S., Ora, A., Olkkonen, V. M., Geng, L., Zerial, M., Somlo, S., and Lehtonen, E. (2000) *J. Biol. Chem.* **275,** 32888–32893

50. Rundle, D. R., Gorbsky, G., and Tsiokas, L. (2004) *J. Biol. Chem.* **279,** 29728–29739

51. Li, Q., Montalbetti, N., Shen, P. Y., Dai, X. Q., Cheeseman, C. I., Karpinski, E., Wu, G., Cantiello, H. F., and Chen, X. Z. (2005) *Hum. Mol. Genet.* **14,** 1587–1603

52. Li, Y., Wright, J. M., Qian, F., Germino, G. G., and Guggino, W. B. (2005) *J. Biol. Chem.* **280,** 41298–41306

53. Philipp, S., Strauss, B., Hirnet, D., Wissenbach, U., Mery, L., Flockerzi, V., and Hoth, M. (2003) *J. Biol. Chem.* **278,** 26629–26638

54. Li, H. S., Xu, X. Z., and Montell, C. (1999) *Neuron* **24,** 261–273

55. Li, Y., Jia, Y. C., Cui, K., Li, N., Zheng, Z. Y., Wang, Y. Z., and Yuan, X. B. (2005) *Nature* **434,** 894–898

56. Bush, E. W., Hood, D. B., Papst, P. J., Chapo, J. A., Minobe, W., Bristow, M. R., Olson, E. N., and McKinsey, T. A. (2006) *J. Biol. Chem.* **281,** 33487–33496

57. Onohara, N., Nishida, M., Inoue, R., Kobayashi, H., Sumimoto, H., Sato, Y., Mori, Y., Nagao, T., and Kurose, H. (2006) *EMBO J.* **25,** 5305–5316

58. Nakayama, H., Wilkin, B. J., Bodi, I., and Molkentin, J. D. (2006) *FASEB J.* **20,** 1660–1670

59. Brenner, J. S., and Dolmetsch, R. E. (2007) *PLoS ONE* **2,** e802

60. Mori, Y., Takada, N., Okada, T., Wakamori, M., Imoto, K., Wanifuchi, H., Oka, H., Oba, A., Ikenaka, K., and Kurosaki, T. (1998) *Neuroreport* **9,** 507–515

61. Goel, M., Sinkins, W. G., Zuo, C. D., Estacion, M., and Schilling, W. P. (2006) *Am. J. Physiol. Renal Physiol.* **290,** F1241–F1252

62. Foggensteiner, L., Bevan, A. P., Thomas, R., Coleman, N., Boulter, C., Bradley, J., Ibraghimov-Beskrovnaya, O., Klinger, K., and Sandford, R. (2000) *J. Am. Soc. Nephrol.* **11,** 814–827

63. Obermüller, N., Gallagher, A. R., Cai, Y., Gassler, N., Gretz, N., Somlo, S., and Witzgall, R. (1999) *Am. J. Physiol.* **277,** F914–F925

64. Bandyopadhyay, B. C., Swaim, W. D., Liu, X., Redman, R. S., Patterson, R. L., and Ambudkar, I. S. (2005) *J. Biol. Chem.* **280,** 12908–12916

65. Roitbak, T., Ward, C. J., Harris, P. C., Bacallao, R., Ness, S. A., and Wandinger-Ness, A. (2004) *Mol. Biol. Cell* **15,** 1334–1346

66. Bai, C. X., Giamarchi, A., Rodat-Despoix, L., Padilla, F., Downs, T., Tsiokas, L., and Delmas, P. (2008) *EMBO Rep.* **9,** 472–479

67. Chang, M. Y., Parker, E., Ibrahim, S., Shortland, J. R., Nahas, M. E., Haylor, J. L., and Ong, A. C. M. (2006) *Nephrol. Dial. Transplant.* **21,** 2078–2084

68. Park, E. Y., Sung, Y. H., Yang, M. H., Noh, J. Y., Park, S. Y., Lee, T. Y., Yook, Y. J., Yoo, K. H., Roh, K. J., Kim, I., Hwang, Y. H., Oh, G. T., Seong, J. K., Ahn, C., Lee, H. W., and Park, J. H. (2009) *J. Biol. Chem.* **284,** 7214–7222

69. Jia, Y., Zhou, J., Tai, Y., and Wang, Y. (2007) *Nat. Neurosci.* **10,** 559–567

70. Kiyonaka, S., Kato, K., Nishida, M., Mio, K., Numaga, T., Sawaguchi, Y., Yoshida, T., Wakamori, M., Mori, E., Numata, T., Ishii, M., Takemoto, H., Ojida, A., Watanabe, K., Uemura, A., Kurose, H., Morii, T., Kobayashi, T., Sato, Y., Sato, C., Hamachi, I., and Mori, Y. (2009) *Proc. Natl. Acad. Sci. U.S.A.* **106,** 5400–5405

71. Shamshirsaz, A. A., Bekheirnia, R. M., Kamgar, M., Johnson, A. M., McFann, K., Cadnapaphornchai, M., Haghighi, N. N., and Schrier, R. W. (2005) *Kidney Int.* **68,** 2218–2224

72. Qian, Q., Hunter, L. W., Li, M., Marin-Padilla, M., Prakash, Y. S., Somlo, S., Harris, P. C., Torres, V. E., and Sieck, G. C. (*2003*) *Hum. Mol. Genet.* **12,** 1875–1880

A Pathogenic C Terminus-truncated Polycystin-2 Mutant Enhances Receptor-activated Ca $^{2+}$ Entry via Association with TRPC3 and TRPC7

Kyoko Miyagi, Shigeki Kiyonaka, Kazunori Yamada, Takafumi Miki, Emiko Mori,
Kenta Kato, Tomohiro Numata, Yuichi Sawaguchi, Takuro Numaga, Toru Kimura,
Yoshikatsu Kanai, Mitsuhiro Kawano, Minoru Wakamori, Hideki Nomura, Ichiro Koni,
Masakazu Yamagishi and Yasuo Mori